THERMOELECTRIC FIGURE OF MERIT OF SINGLE CRYSTALS p-$(Bi_xSb_{1-x})_{2-y}Sn_yTe_3$ IN WIDE TEMPERATURE RANGE

Kulbachinskii V.A.[1], Kytin V.G.[1], Kudryashov A.A.[1], Lostak P.[2]

([1]Low Temperature Physics and Superconductivity Department, Moscow State University M.V. Lomonosov, 119991 GSP-1, Moscow, Russia;

[2]Faculty of Chemical Technology, University of Pardubice, Pardubice, 53210, Czech Republic)

• *Here we report the influence of tin doping on the thermoelectric properties of p-$(Bi_xSb_{1-x})_2Te_3$ single crystals (x = 0; 0.25; 0.5) in the temperature range 7 K – 300 K. Studies of the temperature dependence of Seebeck coefficient S, electrical conductivity σ, heat conductivity k and figure of merit of p-$(Bi_xSb_{1-x})_2Te_3$ single crystals were carried out. In order to determine the concentration of light holes and the Fermi energy, we used the Shubnikov-de-Haas effect at T = 4.2 K. By increasing the Sn content, the hole concentration increases in p-$(Bi_xSb_{1-x})_{2-y}Sn_yTe_3$. The thermal conductivity k of the p-$(Bi_xSb_{1-x})_{2-y}Sn_yTe_3$ crystals decreases due to Sn doping, while electrical resistivity increases in the temperature interval 150 K < T < 300 K and decreases at T < 150 K. The Seebeck coefficient S for all compositions is positive and decreases due to Sn doping in the whole temperature range. The main reason for this is an acceptor effect and increase of the hole concentration under Sn doping. Fermi energy increases with Sn-doping and hence Seebeck coefficient decreases.*

Introduction

Currently, semiconductors based on bismuth and antimony tellurides are the most efficient and widely used materials for thermoelectric devices operating in the temperature range 200 – 350 K. The distortion of the density of states by a resonant impurity of *Sn* was shown to increase the thermoelectric figure of merit *ZT* of the parent semiconductor in the case of Bi_2Te_3 [1]. The concept of an impurity-induced resonant state, also known as a "virtual bound state", was introduced by Friedel [2] as a bound state with a positive energy with respect to the band edge, i.e. with the same energy as an extended state. If it can resonate with a component of that extended state, it builds up two extended states of slightly different energies; these in turn have the same energies as the extended states with whom they will resonate, and so on, until an excess density of states arises over a narrow energy range in the band of the host material. Soon after their discovery, virtual bound states in metals were shown to lead to an increase in thermoelectric power of the host metal by a mechanism now known as resonant scattering [3]. Contrasting with the resonant scattering concept, Mahan and Sofo [4] suggest that the thermopower and the thermoelectric figure of merit can be boosted intrinsically by the excess density of states itself. Because this mechanism does not involve any scattering, it is in essence temperature independent (except for the temperature dependence of the band structure itself [5]), and thus suitable for enhancing the figure of merit in practical thermoelectric materials at and above room temperature. Galvanomagnetic properties of tin-doped solid solutions single crystals $(Bi_xSb_{1-x})_{2-y}Sn_yTe_3$ have been investigated in Ref. [6 – 12]. Quantum oscillations of Hall resistance in a magnetic filed up to 54 T and the energy spectrum of *Sn* doped layered semiconductors p-$(B_{1-x}Sb_x)_2Te_3$ have been studied in Ref. [10, 12]. It is known that tin forms a resonant state 15 meV below the top of the upper valence band and increases the Seebeck coefficient *S* of single crystals of Bi_2Te_3 [6 – 9].

Bi_2Te_3's upper valence bands, UVBs, have Fermi surfaces that consist of six ellipsoidal pockets in *k*-space, centered in the mirror plane of the Brillouin zone lying along 0.3 – 0.5 *X* direction, and have an integral density of states, DOS effective mass $m_d = 0.35m_0$. A lower, heavier valence band, LVB, consisting of six ellipsoids, has been shown to exist 20.5 meV below the UVB in *k*-space at

0.3 – 0.4 A. Bi_2Te_3 can be doped *p*-type with extrinsic atoms such as *Ge*, *Sn*, *Pb*, or *n*-type with *In*, *Cl*, or *I*. Usually, the introduction of doping impurities significantly enhances the thermoelectric power fluctuations, which are due to the stochastic nature of impurity distribution through the crystal. However, the reverse situation is observed for the case of *Sn*-doped Bi_2Te_3. With an increasing amount of the *Sn* impurity, the fluctuations of thermoelectric power and, correspondingly, of the hole concentration decreases, indicating a noticeably improved electrical homogeneity of the crystals [13, 14]. Solid solutions $(Bi_xSb_{1-x})_2Te_3$ are more effective thermoelectric material as Bi_2Te_3. Thus it is important to investigate the influence of *Sn* on thermoelectric figure of merit in the wide temperature range of solid solutions single crystals $(Bi_xSb_{1-x})_2Te_3$ with different *x*. Here we report the influence of tin doping on the thermoelectric properties of $(Bi_xSb_{1-x})_2Te_3$ single crystals in the temperature range 7 K – 300 K. We studied *p*-type single crystal $(Bi_xSb_{1-x})_2Te_3$ (x = 0; 0.25; 0.5) samples both undoped and doped with tin.

Samples

In this work, we investigated pristine and *Sn*-doped *p*-$(Bi_xSb_{1-x})_2Te_3$ (x = 0; 0.25; 0.5) single crystals grown by the Bridgman method. The samples for measurements with characteristic sizes of 1 × 1 × 5 mm (with the largest size along the C_2 axis) after cleavage along the cleavage planes perpendicular to the C_3 axis of the crystal were cut on an electroerosion machine. Electrical contacts were soldered with a *BiSb* alloy. In the measurements of the Hall effect, the current flowed along the C_2 axis and the magnetic field was directed along the C_3 axis. In the measurements of the thermopower and thermal conductivity, the temperature gradient and heat flux were directed along the C_2 axis also. Some parameters of samples according to the galvanomagnetic measurements are listed in Table 1. The actual concentration of tin y in the studied samples was determined experimentally using atomic absorption spectrometry (AAS). As can be seen from Table 1, the Hall hole concentration increases after *Sn* doping. In order to determine the concentration of light holes and the Fermi energy, we also used the Shubnikov-de-Haas effect at T = 4.2 K in high magnetic fields [12].

Table 1

Hall concentration of holes 1/eR, resistivity $\rho_{4.2}$ at T = 4.2 K and ρ_{300} at T = 300 K, Hall coefficient $R_{H4.2}$ and Hall mobility $\mu_{H4.2}$ at T = 4.2 K for $(Bi_{1\,x}Sb_x)_{2-y}Sn_yTe_3$

Sample composition	y – loaded	y-AAS	$1/eR_{H4.2}$ (10^{19}cm^{-3})	$\rho_{4.2}$ (μΩcm)	ρ_{300} (μΩcm)	$\mu_{H4.2}$ (m^2/Vs)	E_F (meV)
$Sb_{2-y}Sn_yTe_3$	0	0	8.2	38.8	260	0.196	104
	0.0075	0.047	56.4	67.6	181	0.018	137
$(Bi_{0.25}Sb_{0.75})_{2-y}Sn_yTe_3$	0	0	6.4	47.4	445	0.205	69
	0.005	0.0030	7.4	68.6	426	0.122	97
	0.0075	0.0034	-	73	292	-	110
$(Bi_{0.5}Sb_{0.5})_{2-y}Sn_yTe_3$	0	0	3.5	56	737	0.320	44
	0.0075	0.0037	20.8	148	435	0.020	115

Thermoelectric properties

1. $Sb_{2-x}Sn_xTe_3$

In Fig. 1 *a* we plot temperature dependence of Seebeck coefficient S for a $Sb_{2-x}Sn_xTe_3$ single crystals. The value of S is positive, hence the both samples (pristine and *Sn*-doped) have *p*-type of conductivity. At low temperatures we see a maximum due to phonon drag. As it is seen in Fig. 1 *a* *Sn*-doping decreases thermoelectric power of Sb_2Te_3 single crystal in the whole temperature interval.

The main reason is that *Sn* is an acceptor and increases the hole concentration and Fermi level.

The simple model with square dispersion law and isotropic relaxation time τ given by

$$\tau = \tau_0 E^r. \tag{1}$$

yields in the following expression for the Seebeck coefficient:

$$S(T) = \frac{k_B}{e}\left(\frac{(2r+5)F_{r+3/2}(\eta)}{(2r+3)F_{r+1/2}(\eta)} - \eta\right), \tag{2}$$

where k_B being Boltzmann constant, e being electron charge, E_F being Fermi energy, $\eta = E_F / k_BT$ is the reduced Fermi energy, and r is a parameter characterizing the scattering mechanism ($r = -1/2$ for acoustic phonon scattering, $r = 1/2$ for polar optical scattering and $r = 3/2$ for ionized impurity scattering);

$$F_s(\eta) = \int_0^\infty [x^s / (e^{x-\eta} + 1)]dx \tag{3}$$

is the Fermi integral. In non degenerating case expression (2) yields for S

$$S = \frac{k_B}{e}\left(p + \frac{5}{2} - \frac{\varepsilon_F}{k_BT}\right). \tag{4}$$

Thus the increase of Fermi energy decreases the value of S.

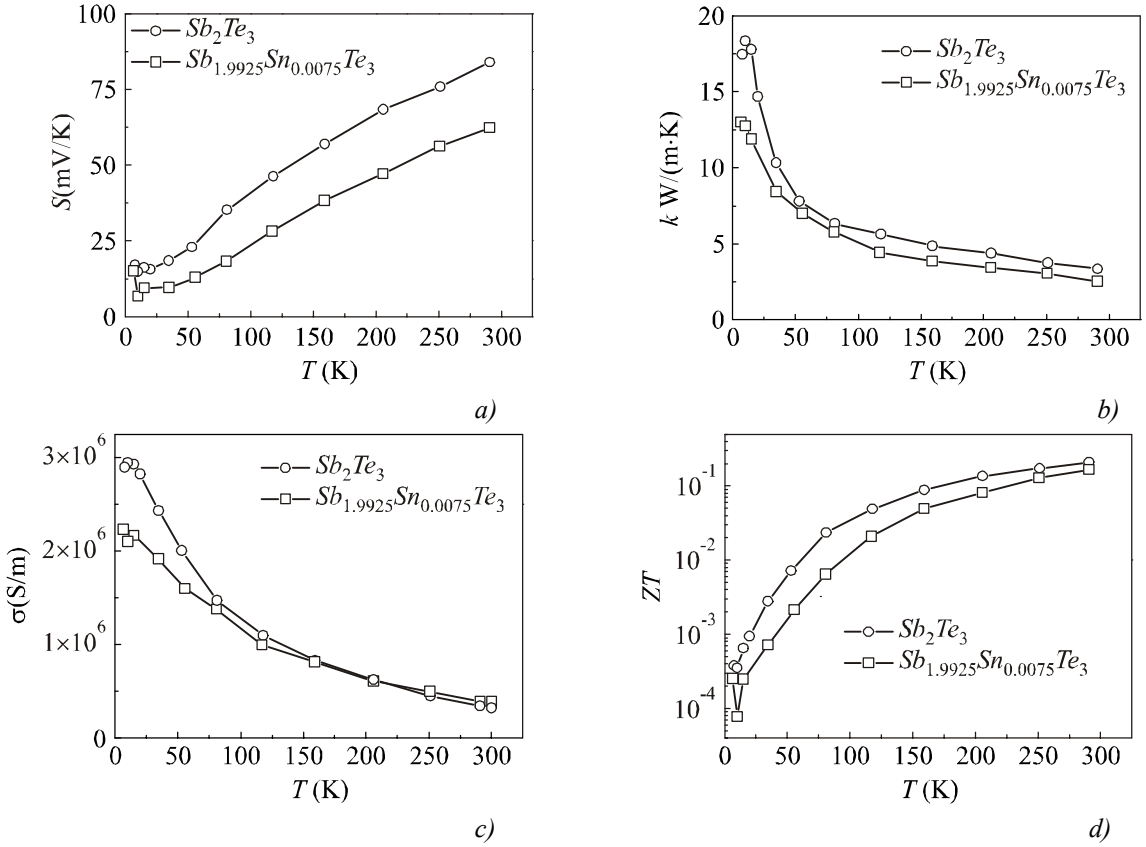

Fig. 1. Temperature dependences of (a) Seebeck coefficient S; (b) thermal conductivity k; (c) the electrical conductivity σ and (d) dimensionless figure of merit ZT for $Sb_{2-x}Sn_xTe_3$ single crystals.

The thermal conductivity of the $Sb_{2-x}Sn_xTe_3$ single crystals were measured in the temperature range 5 – 300 K. The temperature gradient was directed along the C_2 axis. Fig. 1 *b* shows the temperature dependences of of thermal conductivity k. The thermal conductivity k of the $Sb_{2-x}Sn_xTe_3$

crystals decreases insignificantly due to *Sn* doping as compared with pristine Sb_2Te_3, while electrical resistivity increases in the temperature interval 150 K < *T* < 300 K and decreases at *T* < 150 K as it is shown in Fig. 1 *c*. At *T* = 10 K we observed a maximum in *k*(*T*) dependence with value for Sb_2Te_3 about 18 W/m·K. This value is in accordance to observed in Ref. [15, 16]

All these factors lead to the fact that the value of the dimensionless thermoelectric figure of merit *ZT* decreases after tin doping (Fig. 1 *d*).

2. $(Bi_{0.25}Sb_{0.75})_{2-x}Sn_xTe_3$

Temperature dependence of Seebeck coefficient *S* for $(Bi_{0.25}Sb_{0.75})_2Te_3$ and $(Bi_{0.25}Sb_{0.75})_{1.9925}Sn_{0.0075}Te_3$ single crystals are shown in Fig. 2 *a*. The value of *S* is positive and decreases due to *Sn* doping in the whole temperature range. The main reason for this is acceptor effect and increase of the hole concentration under *Sn* doping. Fermi energy increases and according to (2), (4) Seebeck coefficient decrease.

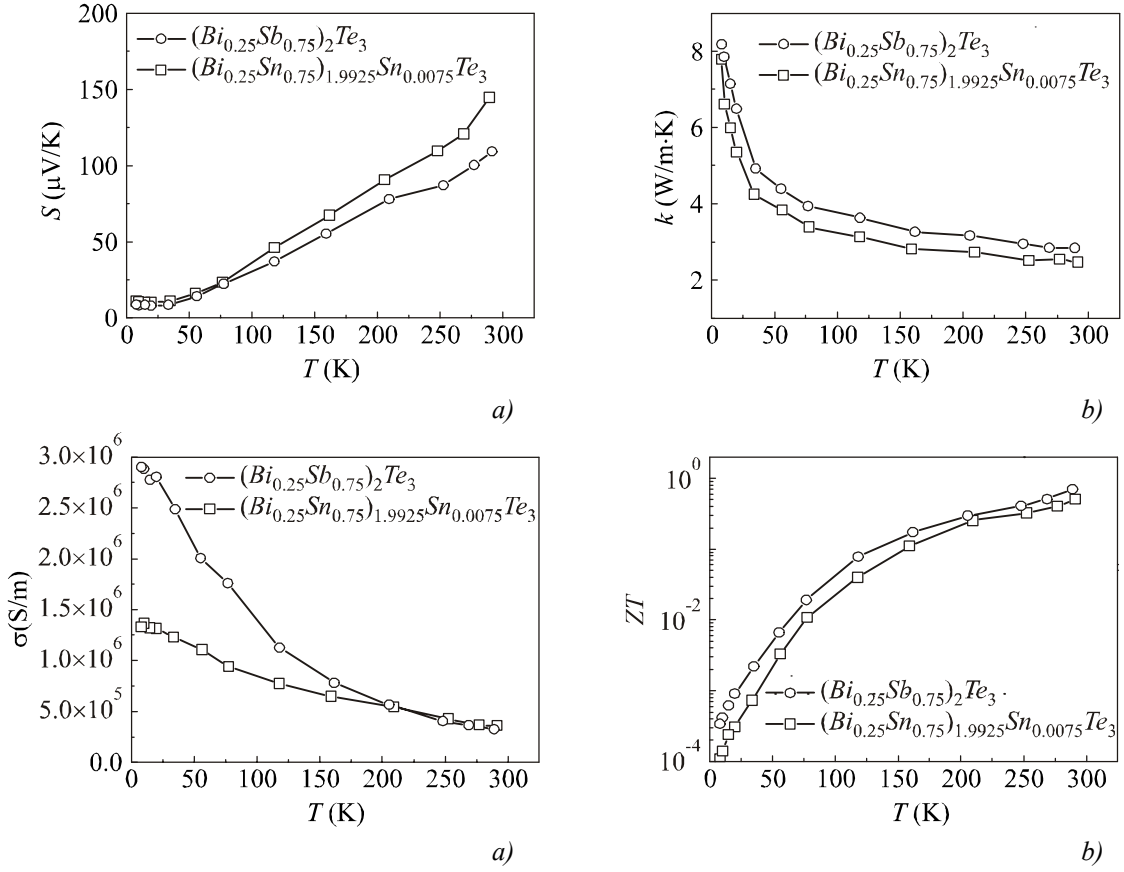

Fig. 2. Temperature dependence of (a) Seebeck coefficient S, (b) thermal conductivity k, (c) electrical conductivity σ, (d) dimensionless thermoelectric efficiency ZT for $(Bi_{0.25}Sb_{0.75})_{2-x}Sn_xTe_3$ single crystals.

The thermal conductivity *k* of $(Bi_{0.25}Sb_{0.75})_2Te_3$ and $(Bi_{0.25}Sb_{0.75})_{1.9925}Sn_{0.0075}Te_3$ single crystals increase up to ~ 8 W/m·K when temperature decreases (Fig. 2 *b*). The value of *k* for $(Bi_{0.25}Sb_{0.75})_{1.9925}Sn_{0.0075}Te_3$ is less than for $(Bi_{0.25}Sb_{0.75})_2Te_3$ in the whole temperature range. It is typical for doped material because of the additional scattering of phonons on impurities. Electrical conductivity increases due to *Sn* doping in the temperature interval 150 K < *T* < 300 K and decreases at *T* < 150 K as it is shown in Fig. 2 *c*. In the whole temperature range it is typical for degenerated conductors, that σ increases with a decrease in temperature. Calculated value of figure of merit *ZT* in *Sn*-doped $(Bi_{0.25}Sb_{0.75})_2Te_3$ is slightly less than in pristine material

as it is shown in Fig. 2 *c*. The main reason for this is decreasing of Seebeck coefficient under *Sn* doping while electrical conductivity at $T > 150$ K even higher in doped samples.

3. $(Bi_{0.5}Sb_{0.5})_{2-x}Sn_xTe_3$

Fig. 3 shows temperature dependences of *S*, *k*, σ and *ZT* for $(Bi_{0.5}Sb_{0.5})_2Te_3$ and $(Bi_{0.5}Sb_{0.5})_{1.9925}Sn_{0.0075}Te_3$ single crystals. The results are similar to that obtained for $(Bi_{0.25}Sb_{0.75})_{2-x}Sn_xTe_3$. Seebeck coefficient *S* and thermal conductivity *k* decrease under *Sn* doping, conductivity increases at $T > 220$ K and decreases at $T < 220$ K. Finally figure of merit *ZT* decreases in the whole temperature range.

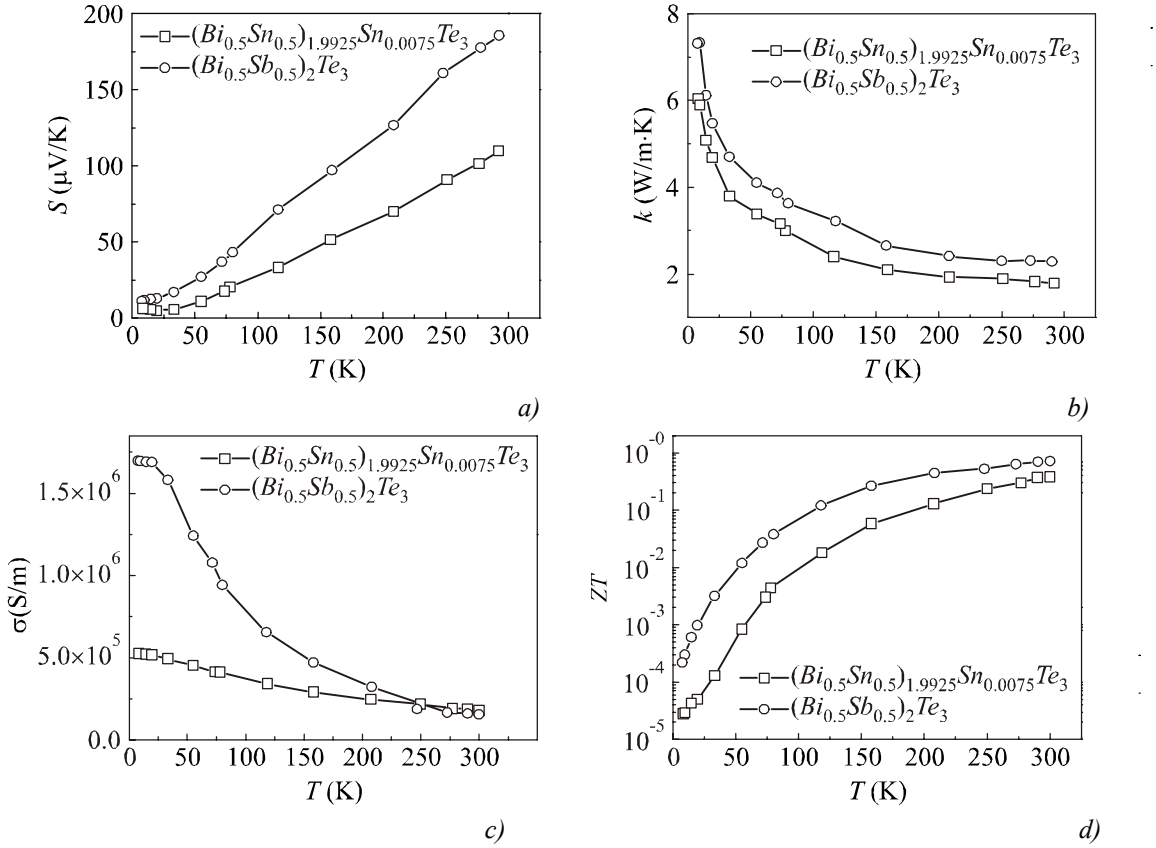

Fig. 3. Temperature dependences of (a) Seebeck coefficient S, (b) thermal conductivity k, (c) electrical conductivity σ, (d) dimensionless thermoelectric efficiency ZT for $(Bi_{0.5}Sb_{0.5})_{2-x}Sn_xTe_3$.

Using simple model with square dispersion law and isotropic relaxation time τ given by (1) we may calculate the scattering parameter *r* using formula (2) for all samples. As an example the value of *r* calculated from experimental data for $(Bi_{0.25}Sb_{0.75})_{2-x}Sn_xTe_3$ is shown in Fig. 4. In *Sn*-free crystals parameter *r* is close to –1/2 at high temperatures indicating the major role of acoustical phonon scattering. At low temperatures *r* increases. Tin doping leads to pronounced increase of *r*. This points to the change of main hole scattering mechanism from acoustic phonon scattering to ionized impurity scattering in doped samples. The same was observed for all investigated solid solutions p-$(Bi_xSb_{1-x})_{2-y}Sn_yTe_3$.

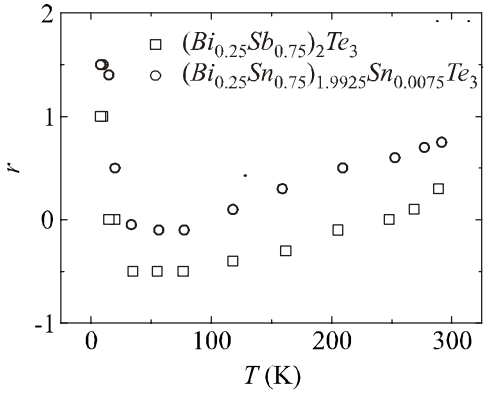

Fig. 4. Temperature dependence of scattering exponent r for $(Bi_{0.25}Sb_{0.075})_{2-y}Sn_yTe_3$ crystals.

Summary

We investigated thermoelectric properties of pristine and *Sn*-doped *p*-$(Bi_xSb_{1-x})_2Te_3$ ($x = 0$; 0.25; 0.5) single crystals in the temperature range $5 < T < 300$ K. We found that tin has an acceptor behavior in solid solutions $(Bi_xSb_{1-x})_2Te_3$. The value of Seebeck coefficient *S* is positive for all composition and decreases due to *Sn* doping in the whole temperature range because of increase of hole concentration in tin-doped samples. Thermal conductivity *k* also decreases due to *Sn* doping for all compositions. The temperature dependence of conductivity σ is more complicated: at room temperature σ increases due to *Sn*-doping while at low temperatures σ decreases. Finally the figure of merit *ZT* decreases at $7 < T < 300$ K for all composition of *p*-$(Bi_xSb_{1-x})_2Te_3$. Preferential scattering mechanism changes in *Sn*-doped samples from acoustic phonon scattering to ionized impurity scattering.

References

1. 1 C.M. Jaworski, V.A. Kulbachinskii, J.P. Heremans, Phys. Rev. B 80, 233201 – 1 (2009).
2. J. Friedel, Can. J. Phys. 34, 1190, (1956).
3. P. de Faget de Casteljau, J. Friedel, J. Phys. Radium, 17, 27 (1956); A. Blandin, J. Friedel, ibid. 20, 160 (1959).
4. G.D. Mahan, J.O. Sofo, Proc. Natl. Acad. Sci. U.S.A. 93, 7436 (1996).
5. V. Jovovic, S.J. Thiagarajan, J.P. Heremans, T. Komissarova, D.R. Khokhlov, A. Nicorici, JAP, 103, 053710 (2008).
6. V.A. Kulbachinskii, N.B. Brandt, P.A. Cheremnykh, S.A. Azou, J. Horak, P. Lostak, Phys. Status Solidi 150, 237 – 243 (1988).
7. V.A. Kulbachinskii, M. Inoe, M. Sasaki, H. Negishi, W.X. Gao, K. Takase, Y. Giman, P. Lostak, J. Horak, Phys. Rev. B 50, 16921-16930 (1994).
8. V.A. Kulbachinskii, H. Negishi, M. Sasaki, Y. Giman, M. Inoue, P. Lostak, J. Horak, Phys. Status Solidi 199, 505 – 513 (1997).
9. V.A. Kul'bachinskii, N.E. Klokova, J. Horak, P. Lostak, S.A. Azou, G.A. Mironova, Sov. Phys. Solid State, 31, 112 – 114 (1989).
10. N. Miyajima, M. Sasaki, H. Negishi, M. Inoue, V.A. Kulbachinskii, A.Yu. Kaminskii, K. Suga, J. Low Temp. Phys. 123, N 3/4, 219 – 238 (2001).
11. Kulbachinskii V.A., Kaminskii A.Yu., Lunin R.A., Kindo K., Narumi Y., Suga K, Kawasaki S., Sasaki S., Miyajima N., G.R. Wu, Lostak P., Hajek, phys. stat. sol. (*b*) 229, 1467 – 1480 (2002).
12. Kulbachinskii V.A., Kaminskii A.Yu., Lunin R.A., Kindo K., Narumi Y., Suga K, Kawasaki S., Sasaki S., Miyajima N., Lostak P., Hajek, Semicond. Sci. Technol. 17, 1133 – 1140 (2002).
13. M.K. Zhitinskaya, S.A. Nemova, V.R. Muhtarova, T.E. Svechnikova, Semiconductors, 45, 988 – 992 (2011).
14. M.K. Zhitinskaya, S.A. Nemov, T.E. Svechnikova, P. Reinhaus, E. Müller, Semiconductors, 34, 1363 – 1364 (2000).
15. P.M. Tarasov, V.A. Kulbachinski, V.G. Kytin, JETP, 105, 21 (2007).
16. Dyck J.S., Chen W., Uher C., Drasar C, Lostak P., Phys. Rev. B., 66, 125206-1 (2002).

Submitted 04.10.2011.